Acta Pharmaceutica Sinica B 2026;16(5):3026−3042

Chinese Pharmaceutical Association
Institute of Materia Medica, Chinese Academy of Medical Sciences

Acta Pharmaceutica Sinica B

www.elsevier.com/locate/apsb
www.sciencedirect.com

ORIGINAL ARTICLE

Curcumin ameliorates metabolic dysfunction-associated steatotic liver disease *via* targeting triokinase/FMN cyclase to regulate the expression of glycerol-3-phosphate acyltransferase 3: Integration of chemical proteomics and transcriptomics

Chongyan Zhao[a,b,c,†], Pan Li[e,†], Jie Shi[a,b,c], Shijie Cao[b,c], Yajing Guo[a,b,c], Gen Li[a,b,*], Ning Kang[b,c,d,*], Feng Qiu[a,b,c,*]

[a]*School of Chinese Materia Medica, Tianjin University of Traditional Chinese Medicine, Tianjin 301617, China*
[b]*Tianjin Key Laboratory of Therapeutic Substance of Traditional Chinese Medicine, Tianjin University of Traditional Chinese Medicine, Tianjin 301617, China*
[c]*State Key Laboratory of Component-based Chinese Medicine, Tianjin University of Traditional Chinese Medicine, Tianjin 301617, China*
[d]*School of Medical Technology, Tianjin University of Traditional Chinese Medicine, Tianjin 301617, China*
[e]*College of Pharmacy, Chongqing Medical University, Chongqing 400016, China*

Received 10 June 2025; received in revised form 9 September 2025; accepted 4 November 2025

KEY WORDS

Curcumin;
MASLD;
Chemical proteomics;
TKFC;
GPAT3;
Lipid metabolism;
Activity-based protein

Abstract Metabolic dysfunction-associated steatotic liver disease (MASLD) is the most common chronic liver disease, posing public health risks from potential irreversible liver damage. Curcumin (Cur), a polyphenolic compound from Zingiberaceae and Araceae, exhibits antihyperlipidemic and insulin-sensitizing effects. However, its targets and mechanisms in MASLD remain unclear. This study aimed to identify the potential targets and mechanisms by which Cur ameliorates MASLD. Cur markedly improved metabolic disorders and inflammation in rats and reduced intracellular lipid accumulation in HepG2 cells, primary hepatocytes, and AML12 cells. TKFC was identified as a direct target of Cur which binds to TKFC at Val136 and Glu538, thereby activating it. Gene microarray screening showed that Cur

*Corresponding authors.
E-mail addresses: ligen0725@163.com (Gen Li), kangndd@163.com (Ning Kang), fengqiu20070118@163.com (Feng Qiu).
[†]These authors made equal contributions to this work.

Peer review under the responsibility of Chinese Pharmaceutical Association and Institute of Materia Medica, Chinese Academy of Medical Sciences.

https://doi.org/10.1016/j.apsb.2026.01.038

profiling;
Triacylglycerol

down-regulated the mRNA expression of *Gpat3*. TKFC knockdown attenuated the down-regulation of GPAT3 by Cur, whereas TKFC overexpression reversed this effect. In *Tkfc*-deficient mice, the therapeutic effects of Cur were attenuated and the down-regulation of GPAT3 and related proteins was hindered, thereby promoting triglyceride production in the liver. Further mechanistic studies revealed that Cur targets TKFC to inhibit GPAT3 expression by modulating the AMPK−STAT3 axis. Our study highlights TKFC as a novel and promising target for MASLD and offers new insights into the molecular mechanisms through which Cur ameliorates MASLD.

1. Introduction

Nonalcoholic fatty liver disease (NAFLD) is now redefined as metabolic dysfunction-associated steatotic liver disease (MASLD), and is associated with obesity, insulin resistance, and dyslipidemia[1]. MASLD encompasses a range of conditions marked by substantial lipid accumulation in the liver without significant alcohol intake, spanning from the milder non-alcoholic fatty liver to the more serious non-alcoholic steatohepatitis[2,3]. Although simple hepatic steatosis is often considered a benign condition, its association with liver fibrosis can progress to cirrhosis and even hepatocellular carcinoma. Current studies indicate that the precise mechanisms underlying the progression of MASLD and its associated complications remain incompletely understood[4]. In 2024, the U.S. Food and Drug Administration approved Resmetirom as the first therapeutic agent for non-alcoholic steatohepatitis, but its clinical application remains associated with certain adverse effects[5]. Therefore, the development of safe and effective intervention strategies is crucial to prevent the malignant progression of MASLD. Carbohydrates and lipids are crucial for energy and cellular functions, with their metabolism precisely regulated by enzymes and receptors to maintain homeostasis; however, prolonged unhealthy dietary habits can disrupt this balance, potentially leading to various metabolic diseases[6,7]. Therefore, restoring and improving impaired metabolic function is considered an effective approach to alleviating MASLD. Lipid metabolic disorders affect several crucial organ systems, particularly the liver, which is not only one of the major insulin-responsive organs, but is also closely associated with lipid accumulation[8,9]. Current therapeutic strategies mainly target well-known metabolic regulators, such as proprotein convertase subtilisin/kexin type 9 and peroxisome proliferator-activated receptors, but their clinical application is often limited by adverse effects[10]. This highlights the need to explore novel, mechanistically distinct targets for safer and more effective metabolic regulation.

The triokinase/FMN cyclase (*TKFC*) gene encodes a bifunctional homodimeric enzyme with triokinase and flavin mononucleotide cyclase activities, consisting of K and L domains. The K domain contains two α/β-folds, and the L domain forms an eight-helix α-barrel. The homodimer adopts an elongated structure (L2−K1−K2−L1). Active sites lie between K1−L2 and K2−L1, where dihydroxyacetone binds K and ATP binds L. Kinase activity requires intact homodimers, while cyclase activity can occur with a truncated single-domain subunit. Triokinase catalyzes the ATP-dependent phosphorylation of D-glyceraldehyde (GA) and dihydroxyacetone, crucial for the final step in the classical HERS pathway of fructose metabolism. Additionally, the cyclizing lyase activity of TKFC could split flavin adenine dinucleotide (FAD) into adenosine monophosphate (AMP) and riboflavin cyclic-4′,5′-phosphate[11]. In the fructose metabolic pathway, fructose-1-phosphate was cleaved by aldolase B into GA and dihydroxyacetone phosphate[12]. Dihydroxyacetone phosphate easily integrates into the glycolytic triose phosphate pool without further metabolism, while GA is phosphorylated by TKFC to glyceraldehyde-3-phosphate and subsequently enters glycolysis[13,14], concluding the final step of fructose breakdown. Jang et al.[15] revealed that TKFC activity might restrict fructose breakdown in certain contexts. In a study by Liu[14], triokinase was considered a metabolic switch that effectively controls lipid synthesis, and triokinase knockout mice exhibited liver inflammation and fructose malabsorption on a high-fructose diet. Analysis of mouse liver proteomic profiles revealed a potential correlation between high TKFC expression and consumption of a high-fat diet[16]. Despite its pivotal role, research on TKFC remains limited, partly because of the absence of recognized clinical conditions correlated with mutations.

The formation of triacylglycerol (TAG) is an essential metabolic process for storing and utilizing energy[17]. This process involves the action of glycerol-3-phosphate acyltransferases (GPATs), which initiate the formation of TAG and glycerophospholipids from glycerol-3-phosphate (G3P)[18]. Currently, four mammalian subtypes of GPATs have been identified: GPAT1 to GPAT4. GPAT1 and GPAT2 are situated in the outer mitochondrial membrane, while GPAT3 and GPAT4 are found in the endoplasmic reticulum (ER)[19,20]. GPATs convert G3P and fatty acyl-CoA into lysophosphatidic acid, which is then transformed into phosphatidic acid by 1-acylglycerol-3-phosphate acyltransferase (AGPAT) using fatty acyl-CoA. Finally, phosphatidic acid phosphohydrolase, also referred to as lipin, facilitates the conversion of phosphatidic acid to diacylglycerol (DAG)[21]. Ultimately, DAG combines with fatty acyl-CoA to form TAG *via* diacylglycerol acyltransferase (DGAT) catalyzes[22]. GPAT3 exhibits predominant expression in tissues characterized by active lipid metabolism. GPAT3 overexpression leads to increased TAG synthesis[23,24]. Thus, GPAT3 could be regarded as a target for managing diseases related to lipid metabolism disorders.

Curcumin (Cur), a diarylheptanoid compound, is present in a variety of traditional Chinese medicines, such as turmeric (*Curcuma longa* L.), Yu Jin (*Curcuma wenyujin* Y. H. Chen et C. Ling), and E Zhu (*Curcuma kwangsiensis* S. G. Lee et C. F. Liang). Owing to its excellent safety, Cur is widely utilized in the food and pharmaceutical industries. In recent years, Cur has gained prominence as one of the "star drugs" due to its diverse biological activities, which include antidiabetic[25], hypolipidemic[26], anti-inflammatory[27], antioxidant[28], and hepatoprotective effects[29]. Orally administered Cur effectively penetrates liver tissues[30], reaching peak levels 2 h after administration[31]. Given the

liver's pivotal role as the "central organ" in lipid metabolism, this accumulation may underpin Cur's efficacy. Previous studies show that Cur could reduce fatty acid synthesis and increase their oxidation by inhibiting acetyl-CoA carboxylase and fatty acid synthase, or activating 5′-AMP-activated protein kinase (AMPK) and peroxisome proliferator-activated receptors[32,33]. Multiple meta-analyses have also confirmed the potential benefits of Cur in patients with MASLD[34,35]. However, it remains unclear which direct target of Cur on the regulation of lipid metabolism to improve MASLD, necessitating further investigation.

In conclusion, the present study integrated transcriptomic and chemical proteomic approaches to systematically screen and identify the direct molecular targets of Cur, with a particular focus on TKFC and its downstream effector GPAT3 in lipid metabolism regulation. Our findings reveal that Cur ameliorates MASLD through the TKFC−GPAT3 axis and suggest that TKFC may serve as a potential pharmacological target of Cur in the treatment of lipid metabolism-related diseases, thereby providing a theoretical basis for the development of novel metabolic interventions.

2. Materials and methods

2.1. Reagents

Cur (purity ≥98%) was from Shanghai Macklin Biochemical Co., Ltd. (Shanghai, China). Protease Inhibitor Cocktail purchased from MedChemExpress (NJ, USA). Total cholesterol (TC), triglyceride (TG), low-density lipoprotein cholesterol (LDL-C), high-density lipoprotein cholesterol (HDL-C), aspartate aminotransferase (AST), alanine transaminase (ALT), nonesterified free fatty acids (NEFA) assay commercially kits obtained from Nanjing Jiancheng Bioengineering Institute (Nanjing, China). Mouse or rat insulin (INS), interleukin (IL)-6 and glucagon-like peptide (GLP)-1 ELISA kits purchased from Cusabio (Wuhan, China). Nitric oxide (NO) assay commercially kits obtained from Beyotime (Shanghai, China). The antibodies for p-AMPK (Thr 172), signal transducer and activator of transcription 3 (STAT3), p-STAT3 were purchased from Cell Signaling Technology (Beverly, MA). The antibodies for DGAT1, AMPK, GPAT3, TKFC, and β-actin were from Proteintech (Wuhan, China). The antibodies for Lipin1, AGPAT1 were from ABclonal (Wuhan, China).

2.2. Cell culture, modeling, and treatment

Human hepatoma HepG2 cells and normal mouse hepatocyte cell line AML12 cells were cultured, serum-starved for 6 h, and treated with 0.5 mmol/L oleic acid (OA) to induce lipid accumulation[36], followed by different concentrations of Cur treatment for 24 h. Primary hepatocytes were isolated from the livers of 8-week-old male C57BL/6 mice, with cell viability assessed by trypan blue exclusion, yielding a viability rate of 92.17%. The cells were treated with OA to induce lipid accumulation and exposed to varying concentrations of Cur treatment. Cell viability was assessed with the MTT assay, and intracellular TG content was measured using a commercial assay kit.

2.3. Oil Red O staining and boron-dipyrromethene (BODIPY) staining

HepG2 cells were fixed and stained with 0.5% oil Red O in isopropanol solution (3:2, *v/v*, Sigma−Aldrich, MO, USA), differentiated in 75% ethanol for 2 min, and finally rinsed thrice with 100 μL of distilled water before imaging. The lipid droplet area was quantified using the ImageJ software. HepG2 cells were incubated with phosphate buffer saline (PBS) buffer (including 5 μmol/L BODIPY and Hoechst 33342 fluorescent dyes) in 96-well plates with opaque side walls and clear bottoms for 30 min. Fluorescence intensity was analyzed using high-content analysis (Cytiva, NY, USA).

2.4. Animals and treatment

Zucker diabetic fatty (ZDF) rats, obtained from Beijing Vital River Laboratory Animal Technology Co., Ltd., were acclimatized to a controlled environment with 12-h light-dark cycles at a constant temperature of 24 ± 2 °C. ZDF (fa/+) rats were fed a normal diet, while ZDF (fa/fa) rats were fed a high-fat diet (HFD). The animals were subsequently divided into six groups: CON (ZDF fa/+, control), MOD (ZDF fa/fa, model), MET (100 mg/kg/day metformin, positive control), Cur-L (curcumin low dose 25 mg/kg/day), Cur-M (curcumin middle dose 50 mg/kg/day), and Cur-H (curcumin high dose 100 mg/kg/day). Each group consisted of eight rats. The oral gavage treatment lasted for four weeks, with weekly recordings of body weight and physiological parameters. Tissue samples were obtained for mRNA and protein determination. Blood samples from all rats were collected from the abdominal aorta for biochemical analyses.

2.5. Biochemistry indexes

Serum TC, TG, LDL-C, HDL-C, AST, ALT, NEFA, IL-6, NO, GLP-1, and INS levels were measured using commercially available kits according to the protocols provided. For the liver TG and TC measurements, tissue extracts were prepared by homogenizing liver tissue in absolute alcohol. The intraperitoneal glucose tolerance test was performed after a 16 h fast using a blood glucose meter (Yuwell, Yancheng, China).

2.6. Cur probe (Cur-P) chemical synthesis

Cur (501 mg, 1.36 mmol/L) was reacted with 3-bromo-1-propyne (162 mg, 1.37 mmol/L) and potassium carbonate (190 mg, 1.37 mmol/L) in 3 mL of dimethylformamide for 48 h under inert gas. The reaction completion was monitored by thin-layer chromatography, followed by quenching with water. Extraction was performed using 10 mL of dichloromethane and removal of residual dimethylformamide was achieved with a saturated sodium chloride solution. The filtrate was concentrated under vacuum to yield a pale-yellow solid. The product was purified using high-performance liquid chromatography (84 mg, 15.1%). MS spectrum and nuclear magnetic resonance (NMR) spectrum of Cur-P showed in Supporting Information Fig. S1. ^{1}H NMR (600 MHz, $CDCl_3$) δ: 7.58 (2H, d, J = 15.5 Hz, H-7, H-13), 7.13 (1H, d, J = 8.8 Hz, H-19), 7.11 (1H, d, J = 8.7 Hz, H-5), 7.08 (1H, s, H-15), 7.04 (1H, s, H-3), 7.03 (1H, d, J = 8.4 Hz, H-18), 6.93 (1H, d, J = 8.1 Hz, H-6), 6.48 (2H, t, J = 15.1 Hz, H-8, H-12), 5.80 (1H, s, H-10), 4.80 (2H, s, H-3′), 3.93 (3H, s, OCH_3), 3.92 (3H, s, OCH_3), 2.54 (1H, s, H-1′); ^{13}C NMR (150 MHz, $CDCl_3$) δ: 181.62 (C-11), 180.76 (C-9), 147.70 (C-17), 146.58 (C-1), 145.87 (C-18), 144.76 (C-6), 138.68 (C-13), 138.02 (C-5), 127.19 (C-4), 125.57 (C-14), 120.87 (C-12), 120.47 (C-8), 119.98 (C-3), 119.69 (C-15), 112.80 (C-16), 111.71 (C-2), 108.35 (C-5), 107.61 (C-19), 99.28 (C-10), 75.99 (C-2′), 74.19 (C-1′), 54.57 (C-3′), 53.90 and

53.89 (C-21/C-20); HR-ESI-MS *m/z*: 407.1516[M+H]$^+$ (calcd. for 407.1495, $C_{24}H_{23}O_6$).

2.7. Click chemistry-activity-based protein profiling (CC-ABPP)

OA-treated HepG2 cell lysates were incubated with dimethyl sulfoxide (DMSO), 10 μmol/L Cur-P, and 10 μmol/L Cur-P plus Cur for 4 h, respectively. A click chemistry reaction cocktail [10 mmol/L biotin azide, 100 mmol/L tris (benzyltriazolylmethyl) amine, 1 mmol/L tris(2-carboxyethyl) phosphine, and 1 mmol/L $CuSO_4$] was added and incubated for 2 h with gentle mixing in the dark, followed by protein precipitation with pre-chilled acetone for 6 h (−20 °C). The harvested proteins were centrifuged, acetone dried, dissolved in PBS with 1.2% sodium dodecyl sulfate.

The samples were pulled down using streptavidin-conjugated beads (Affimag Polystyrene Microspheres Streptavidin) for 4 h, washed with PBS, and separated by sodium dodecyl sulfate-polyacrylamide gel electrophoresis (SDS-PAGE), followed by silver staining. The samples were isolated, trypsin-digested, and identified using liquid chromatography−tandem mass spectrometry (LC−MS/MS) on a Q Exactive mass spectrometer. The MASCOT engine integrated into the Proteome Discoverer 1.4 software was used to search raw data for identification and quantification analysis.

2.8. Western blot analysis

Tissues or cells were lysed with RIPA lysis buffer containing 1 mmol/L protease inhibitor cocktail. The lysates were centrifuged and the concentration was adjusted to 2 mg/mL. The lysates were separated on 6%−15% SDS-PAGE and immunoblotted using the standard protocol[37,38].

2.9. Cellular thermal shift assay (CETSA)

The CETSA was performed according to previously established protocols[39−41]. Cells were collected and lysed. Subsequently, the lysates were partitioned into two aliquots: one subjected to Cur treatment, while the other served as the control (DMSO). These samples were individually subjected to a 3 min heat treatment at various temperatures (40−67 °C), followed by cooling, and then analyzed using Western blotting.

2.10. Drug affinity responsive target stability assay[42,43]

Total protein from HepG2 cells was extracted and diluted, then treated with Cur or DMSO (control). Pronase was added at various concentrations and incubated for 30 min. Samples were analyzed by Western blotting with an anti-TFKC antibody.

2.11. Bio-layer interferometry assay

Recombinant human (rh) TKFC was biotinylated and desalted to remove the unbound biotin. Subsequently, the biotinylated rhTKFC was specifically captured and diluted to a total volume of 400 μL using PBS, employing Super Streptavidin Biosensors (Sartorius, Goettingen, Germany), and immobilized for 1200 s. Upon reaching a signal of 4.5 nm, it was exposed to different concentrations of Cur. The Octet® R8 Protein Analysis System (Sartorius, Goettingen, Germany) was utilized to measure binding and dissociation rates, enabling the calculation of the protein-small molecule affinity.

2.12. Determination of the Cur-binding site on TKFC

rhTKFC was incubated with Cur overnight at 4 °C, then treated with a tris(2-carboxyethyl) phosphine solution at 60 °C for 1 h for reduction. Following this, it was reacted with methyl methylsulfinylmethyl sulfide solution for 45 min. After ultrafiltration and centrifugation, the sample was treated with an 8 mol/L urea solution, washed with 0.25 mol/L tetraethylammonium bromide, and centrifuged. Finally, the filtrate was collected after centrifugation and dried under low-temperature vacuum. Peptide segments were prepared in a solution of 0.1% formic acid and 2% acetonitrile for mass spectrometry analysis. Mass spectrometric data were analyzed using the MASCOT search engine.

2.13. Molecular docking

AutoDock Vina (version 1.1.2) was used for semi-flexible docking, with TKFC as the receptor and Cur as the ligand. Protein structures were obtained from AlphaFold, and Cur structures were obtained from PubChem (CID: 969,516). PyMOL software (version 4.3.0) was used for ligand−protein separation, dehydration, and organic compound removal. AutoDockTools (http://mgltools.scripps.edu/downloads) was used to prepare the protein and ligand structures for docking by hydrogenation, charge checking, and grid box construction. PyMol and Discovery Studio software facilitated the visualization and analysis.

2.14. Cell transfection

HepG2 cells were serum-starved and transfected with *GPAT3* or *TKFC* siRNA using Lipofectamine® 2000 transfection reagent for 6 h. Then, the transfected cells were treated with Cur. The siRNA sequences are listed in Supporting Information Table S1.

2.15. Construction of plasmids and amino acid mutants

Transfection was carried out at 70%−80% confluence of the HepG2 cells using the *GPAT3*-plasmid vector (pIRES2-CMV-*GPAT3*-IRES2-EGFP) or the human *TKFC*-plasmid vector. The site-directed mutant *TKFC* (Val136Ala or Glu538Ala) was cloned into the GV657 vector. The plasmids were constructed using GeneChem (Shanghai, China). The overexpression was performed for 8 h according to the protocol of Lipofectamine® 2000 before the modeling and Cur treatment.

2.16. Adeno-associated virus (AAV) knockdown

The AAV Helper-Free System was used for the knockdown of TKFC in mice liver. The AAV8 vector was generated by co-transfecting three plasmids, including GV687, pAAV-RC, and pHelper in AAV-293 cells and purified *via* CsCl density gradient centrifugation and ultrafiltration. The constructed vector consisted of the following elements in sequence: CMV promoter-EGFP-MIR155 (m*TKFC*)-WPRE-SV40 polyA. C57BL/6 mice were fed high-fat diets (D12492, SPF (Beijing) Biotechnology Co., Ltd.) for 4 weeks to induce lipid metabolism disorder. The AAV particles (1.896×10^{11} v.g) were tail-vein injected into C57BL/6 mice. Subsequently, C57BL/6 mice were treated with Cur orally for 4 weeks. At the end of the experiment, the mice were

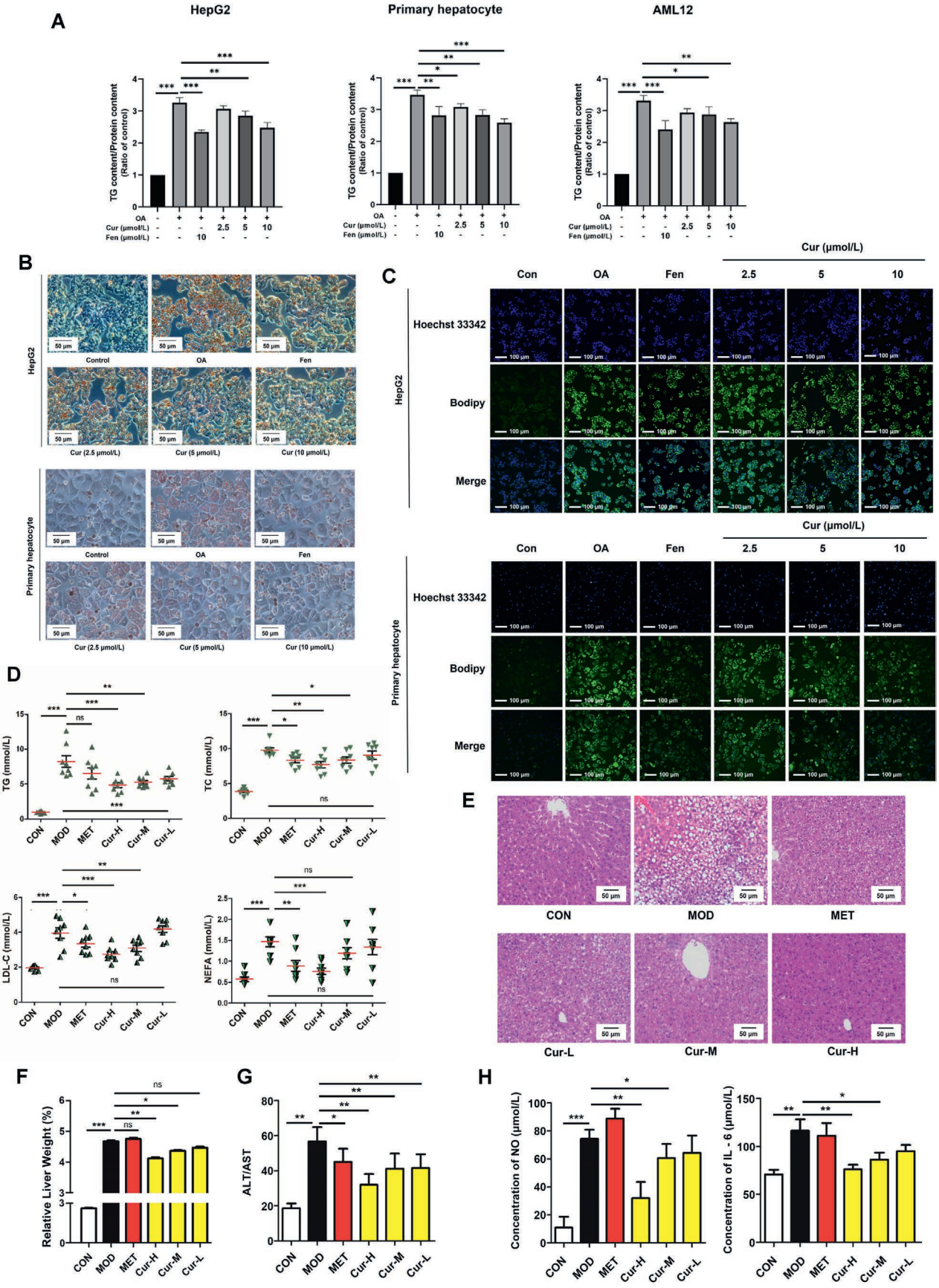
A
HepG2
Primary hepatocyte
AML12
TG content/Protein content (Ratio of control)
OA
Cur (μmol/L)
Fen (μmol/L)
B
HepG2
Primary hepatocyte
Control
OA
Fen
Cur (2.5 μmol/L)
Cur (5 μmol/L)
Cur (10 μmol/L)
C
Cur (μmol/L)
Con
OA
Fen
2.5
5
10
Hoechst 33342
Bodipy
Merge
HepG2
Primary hepatocyte
D
TG (mmol/L)
TC (mmol/L)
LDL-C (mmol/L)
NEFA (mmol/L)
CON
MOD
MET
Cur-H
Cur-M
Cur-L
E
CON
MOD
MET
Cur-L
Cur-M
Cur-H
F
Relative Liver Weight (%)
G
ALT/AST
H
Concentration of NO (μmol/L)
Concentration of IL - 6 (μmol/L)

sacrificed, and the serum biochemical indicators and the expression of key genes and proteins were detected.

2.17. RNA-array

Liver samples were analyzed using an Agilent SurePrint G3 Rat Gene Expression microarray (8 × 60 K, Design ID: 0711,036). Total RNA was extracted, labeled, hybridized, and washed according to the manufacturer's protocol ($n = 5$). Microarray data were analyzed using Feature Extraction (version 10.7.1.1, Agilent Technologies) and Genespring (version 13.1, Agilent Technologies).

2.18. RT-qPCR

Liver RNA was extracted and reverse-transcribed to cDNA using an RNA extraction kit (Tiangen, Beijing, China) and a PrimeScript™ RT reagent Kit (Takara, Tokyo, Japan), followed by RT-qPCR using SYBR Green Master Mix (MedChemExpress, NJ, USA), with results calculated *via* the $2^{-\Delta\Delta Ct}$ method using β-actin as a control, and primer sequences detailed in Supporting Information Table S2.

2.19. Kinase activity assay

TKFC enzymatic activity was assessed using the Kinase-Lumi™ Luminescent Kinase Assay Kit (Beyotime, Shanghai, China). The active reaction system of TKFC was prepared as follows: 50 mmol/L Tris-HCl solution, 10 mmol/L D,L-glyceraldehyde, 0.2 mmol/L ATP, and 0.125 μg human recombinant TKFC protein or 10 μL cell lysate (with 5 mg/mL protein concentration). The reaction was conducted at 25 °C for 10 min, and measurements were taken within 20 min following the manufacturer's guidelines. Enzyme activity was quantified by the reduction in ATP per minute.

2.20. Ethics statement

All experiments involving animals were conducted according to the ethical policies and procedures approved by the Institutional Animal Care and Use Committee of the Tianjin International Joint Academy of Biomedicine (Approval No. TCM-LAEC2023188z1526).

2.21. Statistical analysis

Statistical analysis was conducted using GraphPad Prism 9.5. The results were considered significant at $P < 0.05$. Data are shown as mean ± standard error of the mean (SEM) and were compared using one-way analysis of variance (ANOVA).

3. Results

3.1. Cur ameliorates metabolic disorders in MASLD cells and rats

In OA-treated HepG2, primary hepatocyte, and AML12 cells, Cur showed no obvious toxicity to cell growth when the concentration was below 10 μmol/L (Supporting Information Fig. S2A). Cur treatment significantly reduced intracellular TG levels in a dose-dependent manner (Fig. 1A). Meanwhile, BODIPY and oil Red O staining also demonstrated that Cur could significantly improve cellular lipid accumulation caused by OA (Fig. 1B and C, Fig. S2B-S2E).

ZDF rats were used to establish a MASLD model to confirm the beneficial effects of Cur on the lipid metabolism disorder. We observed that Cur improved the pathological condition with increased diet, water, and excretion (Supporting Information Fig. S3A). Meanwhile, Cur reduced the levels of TC, TG, LDL-C, and NEFA in the serum of the model group (Fig. 1D). H&E staining revealed healthy liver tissue in the CON group, with an intact hepatic structure and orderly hepatic cords around the central vein. In the MOD group, hepatic tissue integrity was disrupted, with disordered hepatic cords and vacuolar changes in some cells, indicating hepatocyte steatosis. In the Cur-treated groups, lipid vacuoles were reduced, and the disrupted hepatic tissue structure showed partial recovery (Fig. 1E). These findings indicate that Cur effectively alleviates liver lipid accumulation. Furthermore, the hepatic index demonstrated a dose-dependent decrease (Fig. 1F), with a notable reduction in liver TG levels observed at higher doses of Cur (Fig. S3B). Cur observably reduced the ALT/AST ratio compared with that in MOD (Fig. 1G), suggesting its potential hepatoprotective effect. Metabolic disorders often involve increased inflammation, as indicated by the elevated NO and IL-6 levels in the MOD group. Unlike metformin, Cur effectively reduced the serum NO and IL-6 levels (Fig. 1H). Notably, fasting blood glucose (FBG) levels significantly decreased during administration, accompanied by a marked reduction in homeostatic model assessment of insulin resistance (Fig. S3C) and an increase in GLP-1 content (Fig. S3D). In addition, Cur also improved the abnormal relative kidney and heart weights (Fig. S3E). These results indicated that Cur could significantly improve metabolic disorders both *in vivo* and *in vitro*.

3.2. Cur down-regulates Gpat3 expression to ameliorate lipid metabolic disorders

In ZDF rats, the RNA array analysis revealed a significant alteration in 357 genes in the MOD group compared to the CON group, with 134 genes being up-regulated and 223 genes being down-regulated. In the Cur-H group, there was a significant modulation of 852 differentially expressed genes compared to the MOD group, with 544 genes up-regulated and 308 genes

Figure 1 Curcumin ameliorates metabolic disorders in both cells and rats with metabolic dysfunction-associated steatotic liver disease. (A) TG content determination in OA-treated HepG2, AML12 and primary hepatocyte cells ($n = 3$). (B) Oil Red O staining in OA-treated HepG2 and primary hepatocyte cells ($n = 3$). (C) BODIPY staining in OA-treated HepG2 and primary hepatocyte cells ($n = 3$). (D) Effects of Cur on blood lipid levels in rats ($n = 8$). (E) Hepatic histopathology ($n = 3$). (F) Relative liver weight in rats ($n = 8$). (G) Determination of the ALT/AST ratio ($n = 8$). (H) Determination of NO and IL-6 levels ($n = 8$). Data are shown as mean ± SEM and compared using one-way ANOVA. $^{*}P < 0.05$, $^{**}P < 0.01$, $^{***}P < 0.001$. ns: not significant.

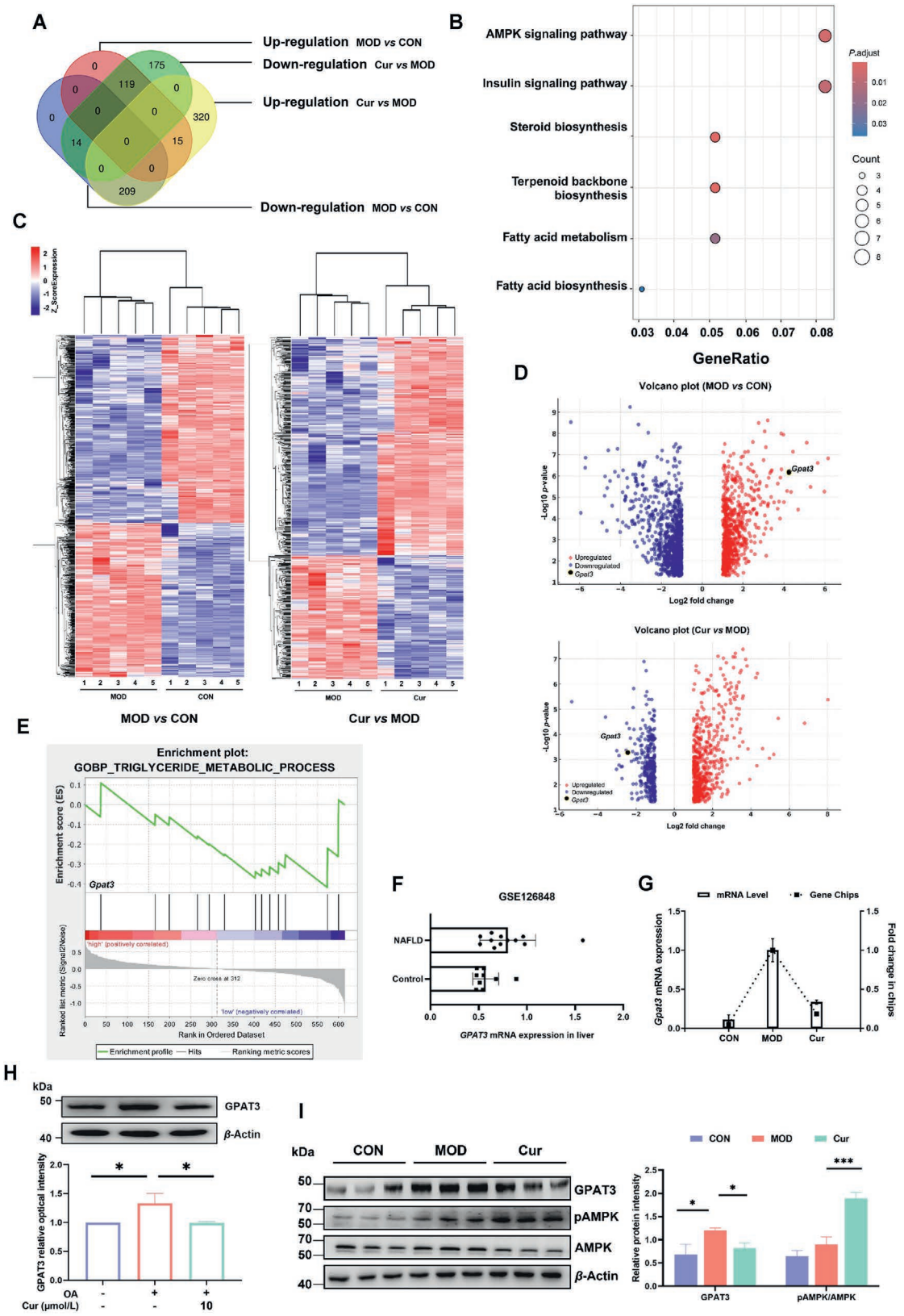

Figure 2 Curcumin improved lipid metabolic disorders by regulating the expression of GPAT3. (A) Statistics of differentially expressed genes in Venn diagram in ZDF rats ($n = 5$). (B) KEGG pathway enrichment analysis of differentially expressed genes ($n = 5$). (C) Cluster analysis of differentially expressed genes. Red represents up-regulation, blue represents down-regulation, and the intensity of color indicates the degree of up-

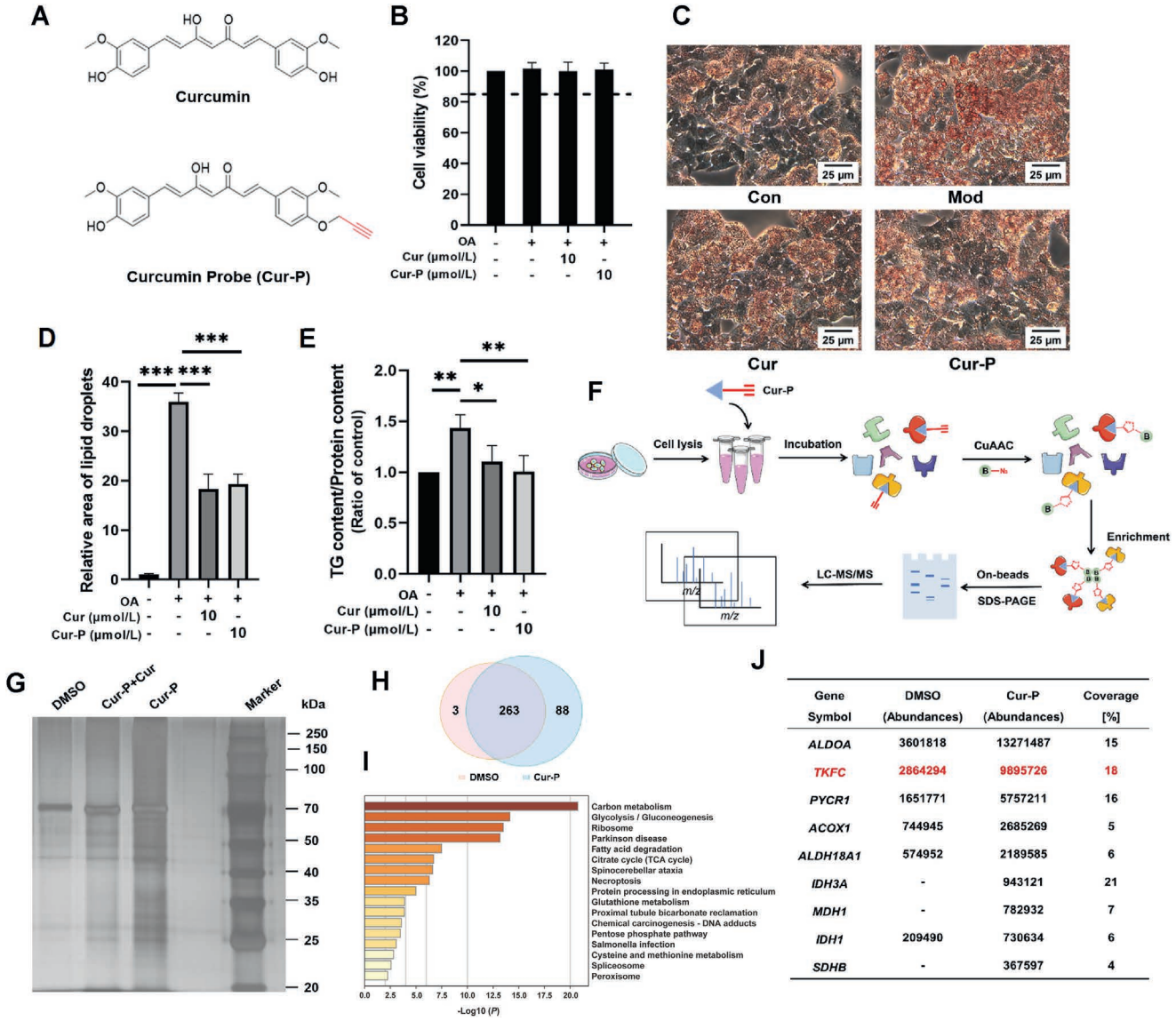

J

Gene Symbol	DMSO (Abundances)	Cur-P (Abundances)	Coverage [%]
ALDOA	3601818	13271487	15
TKFC	2864294	9895726	18
PYCR1	1651771	5757211	16
ACOX1	744945	2685269	5
ALDH18A1	574952	2189585	6
IDH3A	-	943121	21
MDH1	-	782932	7
IDH1	209490	730634	6
SDHB	-	367597	4

Figure 3 Direct target identification of curcumin. (A) Synthesis of the Cur probe. (B) MTT was used to measure the effect of the Cur-P on cell viability ($n = 4$). (C) The effect of Cur-P on lipid droplet accumulation in HepG2 cells was evaluated using oil Red O staining ($n = 3$). (D) Quantitative analysis of oil Red O staining ($n = 3$). (E) Effect of the Cur-P on TG content in HepG2 cells ($n = 3$). Data are shown as mean ± SEM and were compared using one-way ANOVA. $^{*}P < 0.05$, $^{**}P < 0.01$, $^{***}P < 0.001$. (F) Outline of the ABPP strategy for the target identification of small molecule probes in the cells. (G) Cur-P labeled proteome separated by SDS-PAGE and visualized by in-gel fluorescence. (H) Venn diagram showing the number of differentially expressed proteins. (I) KEGG enriched pathways for differential proteins. (J) The table illustrates the ABPP results of nine proteins from carbon metabolism pathways.

down-regulated (Fig. 2A). The intersection of differentially expressed genes in each group was used for Kyoto Encyclopedia of Genes and Genomes (KEGG) pathway enrichment analysis. Notably, the primary signaling pathways influenced by Cur were found to be AMPK and insulin signaling pathways (Fig. 2B). Heatmap clustering analysis indicated noticeable differences in gene expression between each group with relatively good intra-group variation (Fig. 2C). The volcano plot was used to describe

or down-regulation ($n = 5$). (D) Volcano plot analyzed fold change of differential genes in ZDF rats ($n = 5$). (E) GSEA enrichment plot for the triglyceride metabolic process gene set. (F) *GPAT3* mRNA expression in liver tissue from the public dataset. (G) Effect of Cur on *Gpat3* mRNA in the liver of ZDF rats ($n = 5$). (H) Effect of Cur on GPAT3 protein expression in OA-treated HepG2 cells ($n = 3$). (I) Effect of Cur on GPAT3 and AMPK protein expression in the liver of ZDF rats ($n = 3$). Data are shown as mean ± SEM and were compared using one-way ANOVA. $^{*}P < 0.05$, $^{***}P < 0.001$.

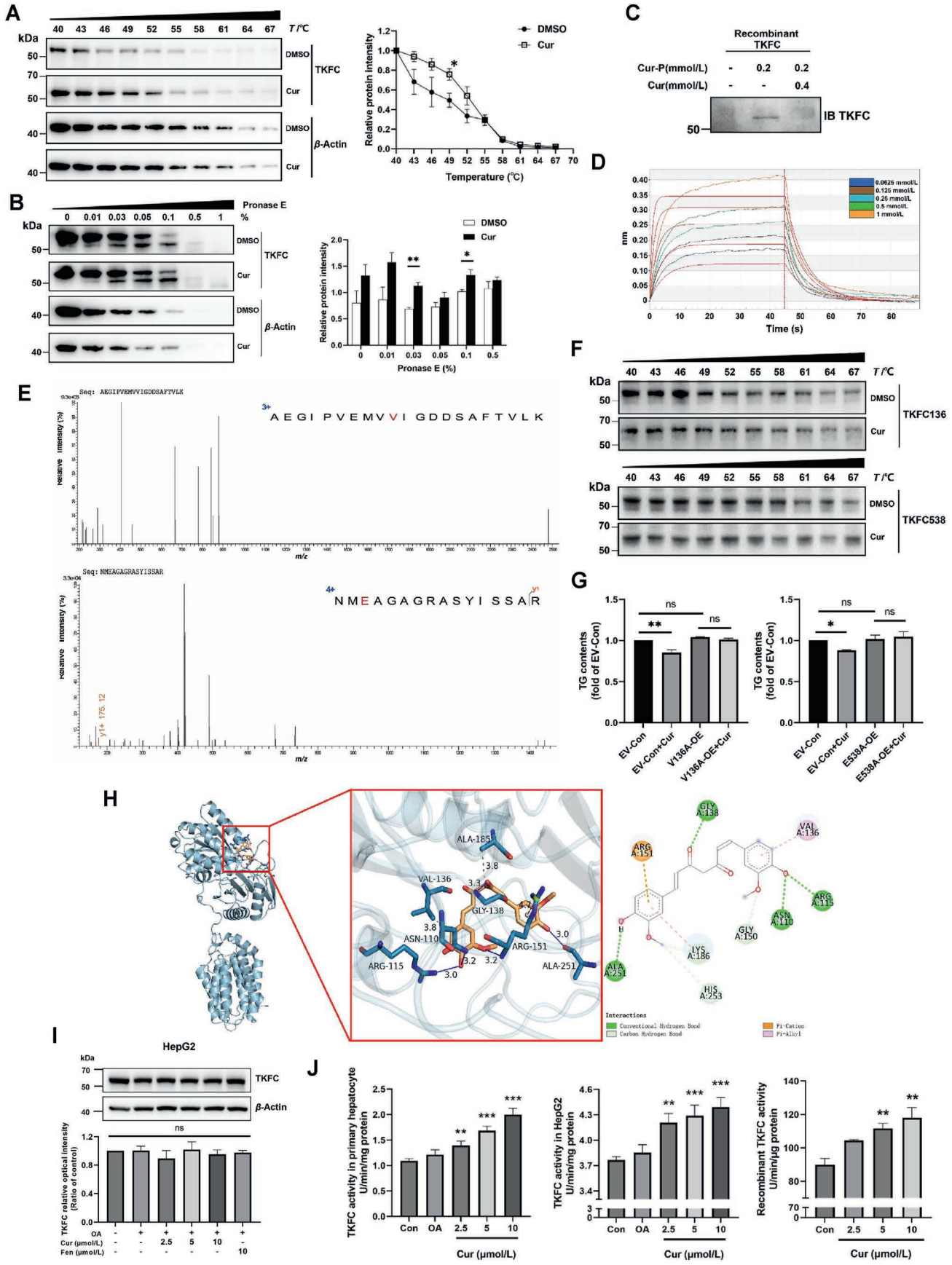
A
B
C
D
E
F
G
H
I
J
TKFC
β-Actin
DMSO
Cur
Pronase E
Recombinant TKFC
IB TKFC
TKFC136
TKFC538
HepG2
Temperature (℃)
Relative protein intensity
Pronase E (%)
Time (s)
TG contents (fold of EV-Con)
EV-Con
EV-Con+Cur
V136A-OE
V136A-OE+Cur
E538A-OE
E538A-OE+Cur
TKFC activity in primary hepatocyte U/min/mg protein
TKFC activity in HepG2 U/min/mg protein
Recombinant TKFC activity U/min/μg protein

the differential RNA expression. It was found that *Gpat3* was significantly up-regulated in MOD, whereas a high dose of Cur significantly down-regulated this gene (Fig. 2D).

Gene Set Enrichment Analysis (GSEA) analysis identified *Gpat3* as the top-ranked gene in the triglyceride metabolic process gene set (Rank Metric Score = 0.341, rank = 37), suggesting a pivotal regulatory role in pathway activation (Fig. 2E). In the Gene Expression Omnibus dataset (GSE126848), hepatic *GPAT3* mRNA expression was significantly upregulated in individuals with NAFLD compared to healthy controls (Fig. 2F). This upregulation suggests that *GPAT3* plays a role in triglyceride accumulation and may contribute to the pathogenesis of NAFLD.

Analysis of the differentially expressed genes based on glucose and lipid metabolism targets revealed that *Gpat3* gene expression was approximately 18-fold higher in the MOD group than in the CON group and decreased approximately 5.4-fold following Cur administration. This trend was validated using RT-qPCR and western blotting analyses on rat liver tissue (Fig. 2G and I). Meanwhile, in an OA-induced lipid accumulation HepG2 cell model, Cur effectively down-regulated the protein expression of GPAT3 (Fig. 2H). AMPK signaling pathways, frequently involved in lipid metabolism, were enriched by KEGG in our study. Western blotting analysis revealed that Cur increased the phosphorylation levels of AMPK in the hepatic tissue of ZDF rats (Fig. 2I). The insulin signaling pathway is also regulated by Cur (Supporting Information Fig. S4A and S4B). Moreover, knockdown of *GPAT3* in HepG2 cells significantly increased glucose consumption and uptake, whereas *GPAT3* overexpression reversed these effects (Supporting Information Fig. S5A−S5F).

3.3. Target profiling of Cur by click chemistry activity-based protein profiling

CC-ABPP is one of the most versatile chemical proteomic methods for compound target discovery[44−46]. To identify the direct targets of Cur, CC-ABPP was employed to map them within a cellular context. An alkyne group was introduced into Cur's hydroxyl position to synthesize an activity-based probe (Cur-P), facilitating its conjugation with biotin for subsequent analysis (Fig. 3A). MTT assay showed that the 10 μmol/L Cur probe had no significant toxicity to OA-treated HepG2 cells (Fig. 3B). We confirmed that the probe retained lipid-lowering activity in HepG2 cells, comparable to that of curcumin (Fig. 3C−E). Next, we performed "click" reactions with Cur-P in cell lysates to label the whole proteome and pull-down/LC−MS/MS-based target identification was employed (Fig. 3F). Silver staining showed that proteins were enriched in the Cur-P group, but decreased in the Cur-P + Cur groups (Fig. 3G). A total of 354 proteins were detected by LC−MS/MS. There were 309 proteins in the probe group whose abundance was more than two times greater than that in the DMSO group, including 88 proteins that were specific to the probe group (Fig. 3H and Supporting Information Table S3). KEGG enrichment analysis indicated that multiple pathways were significantly enriched, with carbon metabolism showing the highest significance (Fig. 3I). In this pathway, TKFC was identified as a prominent candidate, supported by its high confidence scores in protein identification (Fig. 3J). Furthermore, the PPI network showed an interaction between TKFC and GPAT3 (Supporting Information Fig. S6A). Thus, TKFC was prioritized for additional follow-up validation experiments.

3.4. Cur binds directly to TKFC

CETSA and drug affinity responsive target stability experiments were performed in HepG2 cells to verify the interaction between Cur and target proteins. The thermal stability of TKFC was enhanced to varying extents following the addition of Cur at temperatures ranging from 40 to 67 °C (Fig. 4A). Following exposure to Cur, the level of TKFC was significantly elevated compared to the DMSO group when treated with 0.03% and 0.1% pronase E (Fig. 4B), suggesting potential direct interactions between Cur and the TKFC proteins. Furthermore, pull-down western blotting analysis with the corresponding human recombinant protein identified TKFC as a potential target (Fig. 4C). To confirm this finding, Bio-Layer Interferometry analysis was performed with the rhTKFC, revealing a K_d value of 1.38×10^{-4} mol/L for the interaction between Cur and TKFC (Fig. 4D). To determine which amino acid residues were modified by Cur, recombinant TKFC was incubated with Cur, followed by LC−MS/MS analysis. This revealed that Val136 and Glu538 were modified by Cur (Fig. 4E). To validate the binding site of Cur, we mutated Val136 and Glu538 of TKFC to Val136Ala and Glu538Ala, respectively. As shown in Fig. 4F, the thermal stability of the Val136Ala and Glu538Ala mutants was similar to that of the DMSO group. Meanwhile, the mutants reversed the Cur-mediated decrease in TG levels in OA-treated HepG2 cells, indicating that these mutations blocked the binding of TKFC with Cur (Fig. 4G). To further investigate the binding mode of Cur to TKFC, we performed a docking simulation using AutoDock Vina. We found that Cur's stereo conformation fit well with the binding site around the reactive valine residue (Val136), and Cur binds to 136 Val of TKFC by a 3.8 Å hydrophobic binding force (Fig. 4H).

Given the functional importance of this interaction, we next examined whether Cur binding affects TKFC protein expression or enzymatic activity. As shown in Fig. 4I and J, Fig. S6B, TKFC protein expression was not significantly different after Cur treatment. However, Cur promoted the enzymatic activity of TKFC, both in HepG2 and primary hepatocytes, as well as in rhTKFC protein. These findings suggest that the lipid-lowering effect of Cur may be attributed to the functional activation of TKFC.

3.5. Cur targeting TKFC alleviates hepatic lipid metabolism disorder

In HepG2 cells, *TKFC* knockdown reversed the Cur-mediated decrease in TG content and lipid droplet area (Fig. 5A and B,

Figure 4 Curcumin directly binds to Glu538 and Val136 sites of TKFC. (A) Cellular thermal shift assay ($n = 3$). (B) Drug affinity responsive target stability assay ($n = 3$). (C) Pulldown of Cur-P bound rhTKFC proteins. (D) Bio-Layer Interferometry assay. (E) The binding sites of Cur and TKFC amino acid residues were identified by LC−MS/MS. (F) Cellular thermal shift assay was used to detect the direct binding of Cur to mutant proteins. (G) The effect of Cur on TG content was detected by overexpressing the mutant plasmid ($n = 3$). (H) Molecular docking analysis between TKFC protein and Cur. (I) Effect of different concentrations of Cur on TKFC protein expression ($n = 3$). (J) Effect of different concentrations of Cur on cellular TKFC and rhTKFC enzyme activity ($n = 3$). Data are shown as mean ± SEM and were compared using one-way ANOVA. $^*P < 0.05$, $^{**}P < 0.01$, $^{***}P < 0.001$ *vs*. Con. ns: not significant.

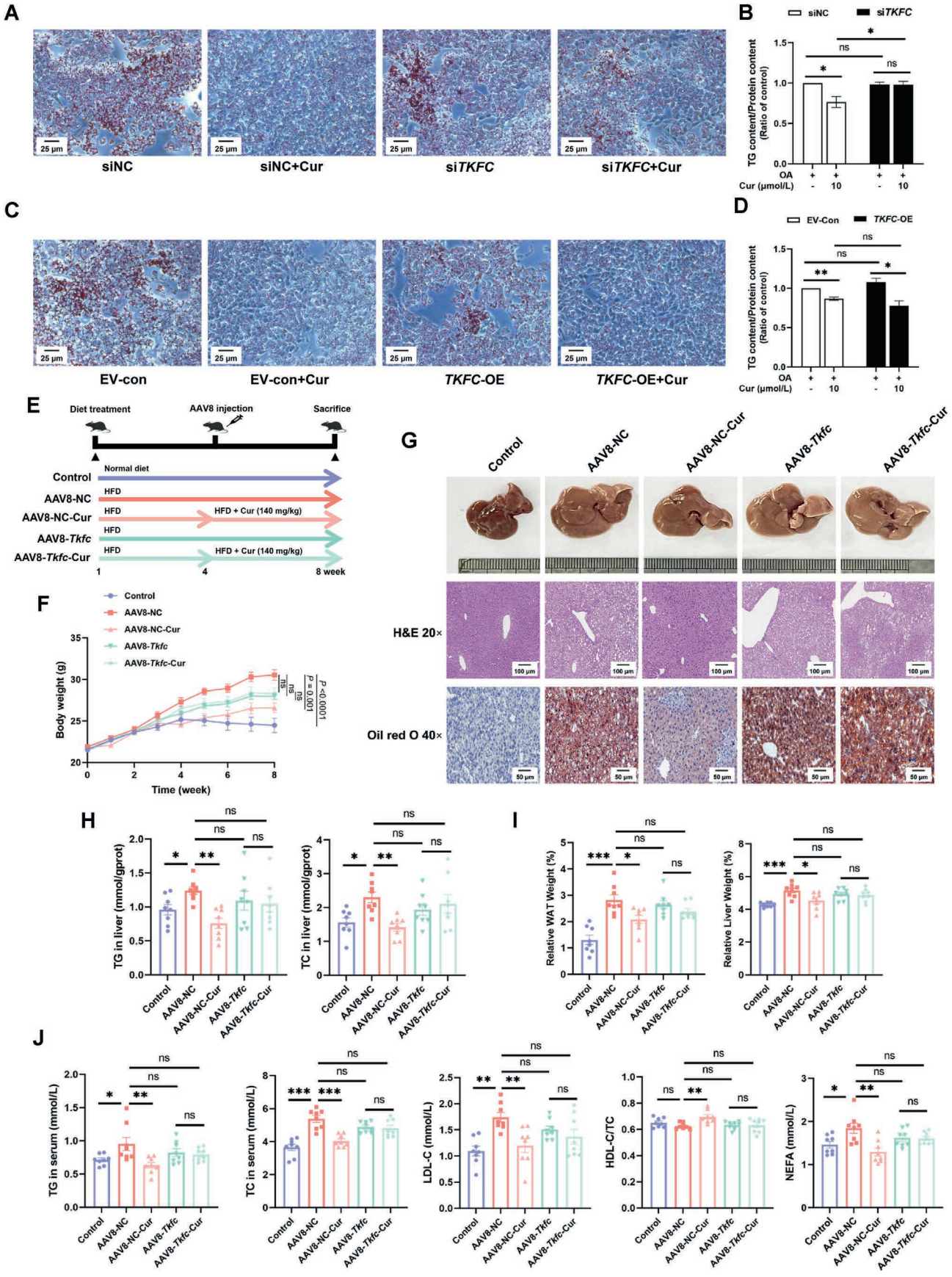
A
siNC
siNC+Cur
siTKFC
siTKFC+Cur
B
siNC
siTKFC
TG content/Protein content (Ratio of control)
OA
Cur (μmol/L)
C
EV-con
EV-con+Cur
TKFC-OE
TKFC-OE+Cur
D
EV-Con
TKFC-OE
E
Diet treatment
AAV8 injection
Sacrifice
Control
AAV8-NC
AAV8-NC-Cur
AAV8-Tkfc
AAV8-Tkfc-Cur
Normal diet
HFD
HFD + Cur (140 mg/kg)
1
4
8 week
F
Body weight (g)
Time (week)
P = 0.001
P <0.0001
G
H&E 20×
Oil red O 40×
H
TG in liver (mmol/gprot)
TC in liver (mmol/gprot)
I
Relative WAT Weight (%)
Relative Liver Weight (%)
J
TG in serum (mmol/L)
TC in serum (mmol/L)
LDL-C (mmol/L)
HDL-C/TC
NEFA (mmol/L)

Fig. S6C). However, Cur treatment significantly reduced TG content and lipid droplet area in HepG2 cells with high *TKFC* expression (Fig. 5C and D, Fig. S6D).

Subsequently, we knocked down the *Tkfc* gene in HFD-fed mice transfected using AAV8 (Fig. 5E). There was an obvious green fluorescence in the liver tissue sections of the AAV group, and the mRNA level of *Tkfc* was decreased significantly (Supporting Information Fig. S7A). In addition, there was no significant effect on TKFC protein expression in the hearts or kidneys of mice (Fig. S7B).

We observed that Cur significantly reduced the body weight of mice compared with those in the AAV8-NC group. However, the weight-reducing effect of Cur was attenuated following *Tkfc* knockdown (Fig. 5F). Liver tissue H&E and oil Red O staining results revealed a significant reduction in the lipid droplet area after Cur administration in AAV8-NC mice, whereas Cur treatment did not exhibit a significant inhibitory effect on hepatic lipid accumulation in the *Tkfc* knockdown model (Fig. 5G and Fig. S7C). Additionally, measurements of liver TG and TC contents indicated a significant attenuation of the therapeutic effects of Cur following *Tkfc* knockdown (Fig. 5H), while Cur had no significant effect on the liver ALT/AST ratio (Fig. S7D). Cur blocked the relative white adipose tissue weight and relative liver weight in AAV8-NC mice, but showed less of an effect in *Tkfc*-deficient mice (Fig. 5I). Similarly, *Tkfc* knockdown reversed the Cur-mediated down-regulation of serum TC, TG, LDL-C, and NEFA, and the up-regulation of the HDL-C/TC ratio in C57BL/6 mice (Fig. 5J). In terms of blood glucose, *Tkfc* knockdown markedly reversed the Cur-regulated decrease in FBG, INS levels, and the HOMA-IR, as well as the increase in glucose tolerance (Fig. S7E and S7F). These results indicate that TKFC is a vital target of Cur in managing metabolism.

3.6. Cur targets TKFC and inhibits GPAT3 expression by regulating the AMPK−STAT3 axis

siRNA-mediated *TKFC* knockdown in HepG2 and AML12 cells clearly ablated the Cur-induced decrease in GPAT3 expression (Fig. 6A, Supporting Information Fig. S8A and S8B). Conversely, we employed *TKFC* overexpression plasmid transfection in HepG2 cells. GPAT3 expression was significantly down-regulated compared to that in the group without Cur (Fig. 6B, Fig. S8C and S8D).

To further identify the relationship between TKFC and GPAT3 *in vivo*, we analyze the effect of *Tkfc* gene silencing on GPAT3 and the related pathway at the mRNA and protein levels. The results showed significant down-regulation of *Gpat3*, *Dgat1*, and *Lipin1* mRNA expression in the Cur-treated control group, whereas the expression of *Gpat3* and *Dgat1* was not regulated by Cur after *Tkfc* knockdown (Supporting Information Fig. S9A). Western blotting showed that Cur inhibited the glycerol phosphate pathway (GPAT3/AGPAT1/Lipin1/DGAT1), thereby reducing TAG generation. However, the inhibitory effect of Cur on the glycerol phosphate pathway was weakened in *Tkfc* knockdown mice (Fig. 6C and Fig. S9B). Pearson correlation coefficient analysis was performed to compare the mRNA expression of *Tkfc* (or *Gpat3*) with serum TG levels in mice. *Tkfc* mRNA levels were not significantly correlated with serum TG levels, whereas *Gpat3* mRNA levels were positively correlated (Fig. 6D). These findings suggest that the effect of Cur on improving the lipid metabolism disorders may be accomplished by targeting TKFC to regulate GPAT3 expression.

Nevertheless, the mechanism by which Cur binds to TKFC regulates GPAT3 remains unclear. To address this, we conducted transcriptomic analysis to investigate the potential impact of *Tkfc* knockdown on hepatic gene expression profiles in mice. As shown in the volcano plot and heatmap (Fig. 6E and Fig. S9C), transcriptome analysis identified 1550 differentially expressed genes. KEGG and GSEA enrichment analyses revealed that the AMPK signaling pathway was notably affected, suggesting that TKFC may regulate lipid metabolism by modulating AMPK activity (Fig. 6F and G). This result is consistent with the findings from the previous liver gene microarray analysis in ZDF rats.

AMPK serves as a central regulator of cellular energy homeostasis and plays a pivotal role in lipid metabolism. AMPK activation leads to decreased lipid accumulation and improved lipid homeostasis. Studies have shown that AMPK activation can inhibit the phosphorylation of STAT3, thereby suppressing its transcriptional activity[47,48]. Since STAT3 acts as a transcription factor for GPAT3[49], it is speculated that the changes in GPAT3 expression may be mediated by the AMPK−STAT3 axis. Immunofluorescence results showed that Cur treatment significantly reduced the nuclear localization of STAT3, an effect that was abolished in *TKFC* knockdown cells (Fig. 6H). Additionally, a dual-luciferase reporter gene system was constructed, demonstrating that *STAT3* can regulate the transcription of *GPAT3* (Fig. 6I). Western blot analysis showed that in both cells and mice, Cur significantly activated AMPK and inhibited the phosphorylation of STAT3. However, these effects were attenuated in cells with *TKFC* knockdown, suggesting that Cur inhibits GPAT3 expression by targeting TKFC to regulate the AMPK−STAT3 axis (Fig. 6J and K, Fig. S9D−S9F).

4. Discussion

The pathogenesis of MASLD is highly complex, involving various factors including lipid metabolism disorders, insulin resistance, and inflammation. The interaction between disordered lipid metabolism and the resulting inflammatory response could together drive the occurrence and progression of MASLD. Cur is considered to be a pleiotropic natural product, and has been frequently reported in MASLD, obesity and T2DM treatment over

Figure 5 Curcumin improves lipid accumulation by targeting TKFC in cells and mice. (A) Effect of Cur on lipid accumulation in *TKFC* knockdown OA-treated HepG2 cells ($n = 3$). (B) Effect of Cur on TG level in *TKFC* knockdown OA-treated HepG2 cells ($n = 3$). (C) Effect of Cur on lipid accumulation in OA-treated HepG2 cells with a *TKFC* overexpression ($n = 3$). (D) Effect of Cur on TG level in OA-treated HepG2 cells with a *TKFC* overexpression ($n = 3$). (E) Experimental procedure of AAV8 transfection in C57BL/6 mice. (F) Effects of Cur on weight of *Tkfc* gene knockdown mice ($n = 8$). (G) The liver sizes and hepatic steatosis as measured by H&E and oil Red O staining ($n = 3$). (H) Effects of Cur on TG and TC in livers of *Tkfc* gene knockdown mice ($n = 8$). (I) Effects of Cur on liver and white adipose tissue (WAT) relative weight in *Tkfc* gene knockdown mice ($n = 8$). (J) Effects of Cur on blood lipid levels in *Tkfc* gene knockdown mice ($n = 8$). Data are shown as mean ± SEM and were compared using one-way ANOVA. $^{*}P < 0.05$, $^{**}P < 0.01$, $^{***}P < 0.001$. ns: not significant.

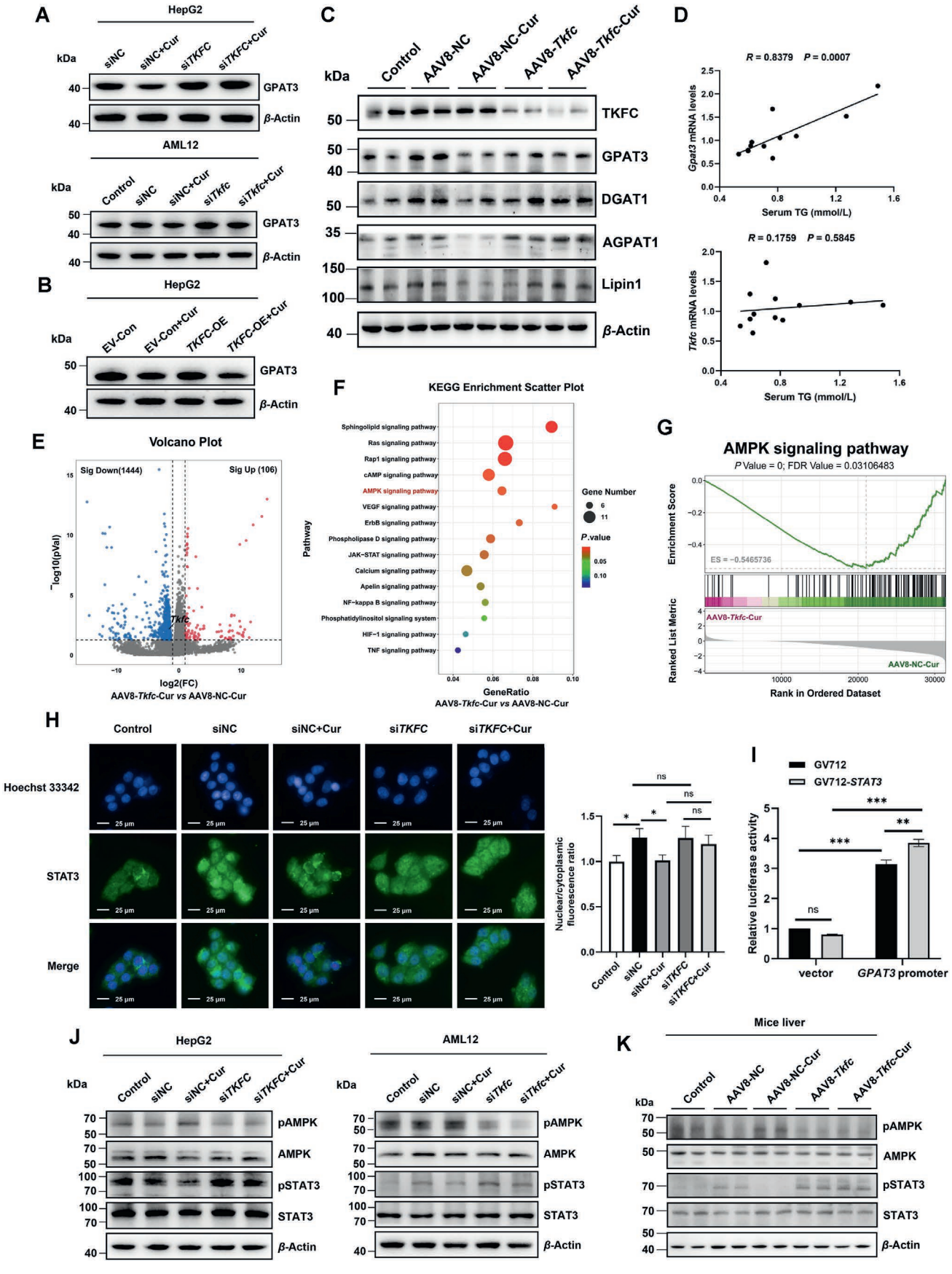
A
HepG2
kDa
siNC
siNC+Cur
siTKFC
siTKFC+Cur
40
GPAT3
40
β-Actin
AML12
kDa
Control
siNC
siNC+Cur
siTkfc
siTkfc+Cur
50
40
GPAT3
40
β-Actin
B
HepG2
kDa
EV-Con
EV-Con+Cur
TKFC-OE
TKFC-OE+Cur
50
GPAT3
40
β-Actin
C
kDa
Control
AAV8-NC
AAV8-NC-Cur
AAV8-Tkfc
AAV8-Tkfc-Cur
50
TKFC
50
40
GPAT3
50
DGAT1
35
AGPAT1
150
100
Lipin1
40
β-Actin
D
R = 0.8379 P = 0.0007
Gpat3 mRNA levels
Serum TG (mmol/L)
R = 0.1759 P = 0.5845
Tkfc mRNA levels
Serum TG (mmol/L)
E
Volcano Plot
Sig Down(1444)
Sig Up (106)
Tkfc
−log10(pVal)
log2(FC)
AAV8-Tkfc-Cur vs AAV8-NC-Cur
F
KEGG Enrichment Scatter Plot
Sphingolipid signaling pathway
Ras signaling pathway
Rap1 signaling pathway
cAMP signaling pathway
AMPK signaling pathway
VEGF signaling pathway
ErbB signaling pathway
Phospholipase D signaling pathway
JAK−STAT signaling pathway
Calcium signaling pathway
Apelin signaling pathway
NF−kappa B signaling pathway
Phosphatidylinositol signaling system
HIF−1 signaling pathway
TNF signaling pathway
Pathway
GeneRatio
Gene Number
P.value
AAV8-Tkfc-Cur vs AAV8-NC-Cur
G
AMPK signaling pathway
P Value = 0; FDR Value = 0.03106483
Enrichment Score
ES = −0.5465736
AAV8-Tkfc-Cur
AAV8-NC-Cur
Ranked List Metric
Rank in Ordered Dataset
H
Control
siNC
siNC+Cur
siTKFC
siTKFC+Cur
Hoechst 33342
STAT3
Merge
25 μm
Nuclear/cytoplasmic fluorescence ratio
ns
I
GV712
GV712-STAT3
Relative luciferase activity
vector
GPAT3 promoter
J
HepG2
AML12
kDa
Control
siNC
siNC+Cur
siTKFC
siTKFC+Cur
siTkfc
siTkfc+Cur
pAMPK
AMPK
pSTAT3
STAT3
β-Actin
K
Mice liver
kDa
Control
AAV8-NC
AAV8-NC-Cur
AAV8-Tkfc
AAV8-Tkfc-Cur
pAMPK
AMPK
pSTAT3
STAT3
β-Actin

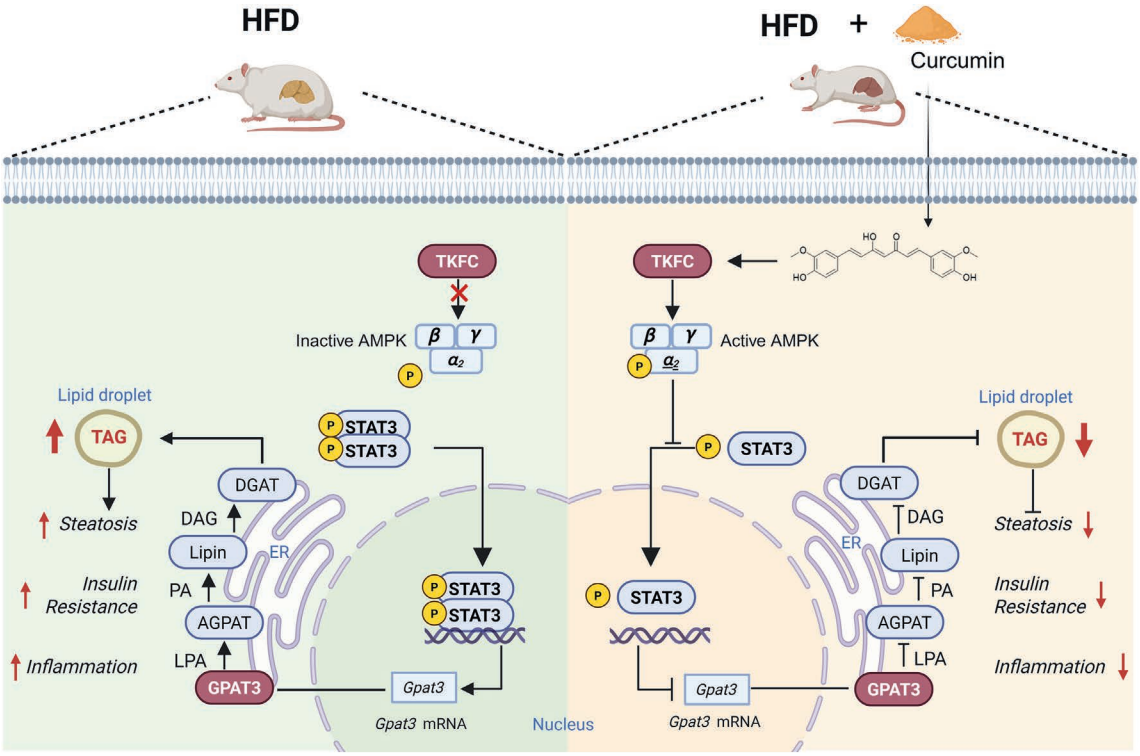

Figure 7 The potential molecular mechanism of Cur in alleviating MASLD.

recent decades[26,35,50]. Although some studies have questioned its specificity, subsequent articles published in Nature refuted this view and reaffirmed the biological effects of Cur[51,52]. In our study, abnormal glycolipid indicators, including TG, TC, LDL-C, FFA, FBG, etc., were improved by Cur administration for 4 weeks. In addition, the treatment effect of 100 mg/kg/day Cur is better than that of equivalent metformin. As a proven anti-inflammatory and antioxidant natural product, Cur has been demonstrated to be effective in reducing NO and IL-6 levels, which alleviates the negative effects of lipid metabolism disorders to a certain extent. Although Cur exhibits significant biological effects, its clinical application still relies on further optimization of its bioavailability. By developing more effective delivery systems and optimizing Cur formulations, its clinical value, particularly in the treatment of MASLD and other metabolic diseases, can be significantly enhanced.

Ectopic lipid accumulation is an important risk factor for MASLD. These accumulated lipids assemble excessively in the hepatic tissues and ultimately cause hepatic steatosis[53]. The fatty acid pathway and channels involved in TG synthesis are highly compartmentalized. Fatty acids are activated and attached to G3P in the ER, leading to the formation of the lipid intermediate DAG, which can be further esterified to TGs in subsequent reactions[54,55]. Therefore, the continuous formation of TGs contributes to the formation of ER-derived lipid droplets, which are dispersed subcellular organelles involved in various cellular processes beyond the storage of neutral lipids[56]. In recent years, numerous genome-wide studies have identified multiple polymorphisms in genes associated with MASLD susceptibility. GPAT3 is an important enzyme located in the ER, which has been confirmed to possess both AGPAT and GPAT activities that control the synthesis of TGs[18]. Chen et al.[57] reported that Asiatic acid inhibited *GPAT3* mRNA expression, thereby affecting the biosynthesis of metabolites such as 1-acyl-*sn*-glycerol-3-phosphocholine, phosphatidylcholine, phosphatidylethanolamine, and phosphatidylserine, which regulate the glycerophospholipid metabolism pathway, ultimately ameliorating alcoholic hepatitis. Furthermore, *N*-acetylcysteine could reverse HFD-induced *Gpat3* mRNA high-

Figure 6 Curcumin targets TKFC and inhibits GPAT3 expression by regulating the AMPK−STAT3 axis. (A) Effect of Cur on GPAT3 expression in *TKFC* knockdown HepG2 and AML12 cells ($n = 3$). (B) Effect of Cur on GPAT3 expression in OA-treated HepG2 cells with a *TKFC* overexpression ($n = 3$). (C) Effects of Cur on glycerol phosphate metabolic pathways of protein expression in *Tkfc* gene knockdown mice ($n = 4$). (D) Pearson correlation analysis between *Tkfc* and *Gpat3* mRNA expression and mice serum TG levels. (E) Volcano plot showing differential expressed genes between AAV8-*Tkfc*-Cur and AAV8-NC-Cur groups ($n = 4$). (F) KEGG pathway enrichment scatter plot displaying significantly enriched signaling pathways ($n = 4$). (G) GSEA plot showing the enrichment of the AMPK signaling pathway between the AAV8-*Tkfc*-Cur and AAV8-NC-Cur groups ($n = 4$). (H) The effect of Cur on STAT3 nuclear localization in *TKFC* knockdown cells ($n = 3$). (I) Dual-luciferase reporter assay was employed to investigate the regulatory effect of STAT3 on the GPAT3 promoter. The GPAT3 promoter and a negative control (CON) were cloned into the GV534 vector, while the STAT3 cDNA was inserted into the GV712 vector to construct an overexpression plasmid. HEK293T cells were co-transfected with a STAT3 expression plasmid together with the GPAT3 promoter-firefly luciferase and *Renilla* control vectors, and luciferase activity was measured 48 h post-transfection ($n = 3$). (J) Expression of AMPK−STAT3 axis protein in *TKFC* knockdown HepG2 and AML12 cells ($n = 3$). (K) Expression of AMPK−STAT3 axis protein in *Tkfc* gene knockdown mice ($n = 4$). Data are shown as mean ± SEM and were compared using one-way ANOVA. $^*P < 0.05$, $^{**}P < 0.01$, $^{***}P < 0.001$. ns: not significant.

expressed to alleviate hepatic steatosis and injury[58]. In our study, we found that the mRNA level of *Gpat3* increased 18-fold in ZDF rats compared to that in ZDF normal rats by microarray analysis, and Cur treatment caused a 5.4-fold decrease compared to that in the MOD group. These results indicate that GPAT3 may be a regulator of lipid metabolism and a key protein in Cur treatment.

Current methods based on ABPP have undergone systematic exploration and review to develop standardized tools to identify and functionally characterize individual proteins from complex proteomes[59−62]. A characteristic of ABPP is the design of small-molecule probes that can modify the active sites of proteins[63]. Once protein covalent modification is achieved, the reporter groups on the probes allow the visualization or isolation of labeled proteins through various methods[64−66]. TKFC is a bifunctional enzyme involved in the ATP-dependent phosphorylation of GA and dihydroxyacetone during fructose metabolism. Its kinase activity depends on the binding of substrates and ATP to distinct domains on separate subunits, with phosphate group transfer facilitated by specific conformational changes[11]. This process may require conformational modulators such as FAD to stabilize the enzyme's catalytic configuration. Our study found that Cur did not significantly alter the protein expression level of TKFC but enhanced its enzymatic activity in a dose-dependent manner. This suggests that Cur may promote conformational transitions of TKFC through an allosteric regulatory mechanism, thereby activating its catalytic function. Further mechanistic investigation revealed that Cur activates TKFC to regulate the downstream AMPK−STAT3−GPAT3 signaling pathway, ultimately inhibiting triglyceride synthesis. Therefore, the regulatory role of TKFC in lipid metabolism appears to depend on Cur-induced activation of its enzymatic function rather than changes in its protein abundance. Activation of TKFC lies at a strategic node of the hepatic Hers pathway. By accelerating ATP-dependent phosphorylation of D-glyceraldehyde/dihydroxyacetone and cleaving FAD to AMP, TKFC activation is expected to raise the AMP/ATP ratio and engage AMPK signaling[67], linking to our observations of AMPK activation, reduced STAT3 activity, and GPAT3 down-regulation. Under TKFC activation, increased triose flux may augment glycolytic throughput and lactate production, thereby altering the cytosolic redox state[68]. It could also disturb glyceraldehyde levels, leading to transient accumulation that may impact cell viability[69]. However, these effects are theoretical speculations, and their actual occurrence and severity are highly dependent on the extent of TKFC activation, physiological conditions (such as exposure to a high fructose diet), and the overall balance of metabolic pathways, etc. Within the Cur dose range used in this study (cells: 2.5−10 μmol/L, rats: 25−100 mg/kg/day), we observed no overt fructose-related toxicity.

Our results showed that Cur binds to Val136 and Glu538 of TKFC, located in the K and L domains, respectively, which may influence the enzymatic activity of TKFC. The covalent modification observed at Glu residues may suggest the involvement of oxidative activation, such as the formation of Cur-derived quinone intermediates, which could react with nucleophilic oxygen centers or participate in radical-mediated crosslinking. Although Glu is not typically considered a reactive residue, esterification or atypical rearrangement mechanisms under oxidative or dehydrating conditions may explain this modification. The detection of covalent modification at valine residues is unexpected, given the lack of nucleophilic side chains. While this may reflect a misassignment or modification of neighboring residues, it is also possible that under oxidative stress conditions, non-specific radical-induced crosslinking occurred at hydrophobic sites. However, molecular docking results identified Val136 as a binding site for Cur. Therefore, we hypothesize that the interaction is driven by hydrophobic forces rather than covalent bonding[70].

AMPK is a central energy sensor that regulates lipid and glucose metabolism. Activation of AMPK promotes catabolic pathways while inhibiting anabolic processes. Structurally, AMPK is a heterotrimer composed of a catalytic α subunit and regulatory β and γ subunits. The α subunit contains an N-terminal kinase domain, whose activity depends on phosphorylation of the conserved Thr172 residue within the activation loop near the ATP-binding site. Phosphorylation at Thr172 is widely used as a marker of AMPK activation[71,72]. Activation of AMPK inhibits STAT3 nuclear translocation and promotes its cytoplasmic phosphorylation, thereby reducing the transcriptional activity of STAT3. STATs are a special family of DNA-binding proteins. In resting cells, STAT proteins are predominantly localized in the cytoplasm. Upon activation, STAT molecules form dimers and translocate into the nucleus. STATs contain SH2 and SH3 domains, which enable them to bind to specific phosphotyrosine-containing peptide motifs. Upon phosphorylation, STAT proteins dimerize to form active transcription factors that migrate into the nucleus, where they bind to the promoter regions of target genes and promote their transcription. Recent studies have shown that STAT3 can bind to the promoter region of GPAT3, thereby enhancing its transcriptional activity[73]. In studies related to fatty acid metabolism, STAT3 has also been observed to regulate the fatty acid esterification process by inhibiting GPAT3 activity[74].

5. Conclusions

Cur can ameliorate glucose and lipid metabolism disorders both *in vivo* and *in vitro*. We identified TKFC as a direct target of Cur, which downregulates GPAT3 expression by modulating the AMPK−STAT3 axis and inhibits the glycerol phosphate pathway (Fig. 7). These results enhance our understanding of lipid metabolism regulation and offer new therapeutic approaches for MASLD. Further investigation into the interaction between Cur and TKFC is necessary to develop more targeted clinical strategies for treating lipid metabolism disorders.

Acknowledgments

This work was supported by the National Natural Science Foundation of China (Nos. 82430120 and 82074281, China) and National Key Research and Development Program of China (No. 2025YFE0212400, China).

Author contributions

Feng Qiu, Ning Kang and Gen Li: Resources, Conceptualization, Supervision, Funding acquisition, Writing - Review & Editing. Chongyan Zhao: Writing - Original Draft, Methodology, Data Curation. Pan Li: Visualization, Writing-original draft. Jie Shi: Methodology, Investigation. Shijie Cao: Writing - Review & Editing, Methodology. Yajing Guo: Formal analysis, Validation.

Conflicts of interest

The authors have no conflicts of interest to declare.

Appendix A. Supporting information

Supporting information to this article can be found online at https://doi.org/10.1016/j.apsb.2026.01.038.

References

1. Hsu CL, Loomba R. From NAFLD to MASLD: implications of the new nomenclature for preclinical and clinical research. *Nat Metab* 2024;**6**:600−2.
2. Zhang Y, Chen Y. Roles of organelle-specific autophagy in hepatocytes in the development and treatment of non-alcoholic fatty liver disease. *Chin Med J (Engl)* 2022;**135**:1673−81.
3. Fang Z, Shen G, Wang Y, Hong F, Tang X, Zeng Y, et al. Elevated kallistatin promotes the occurrence and progression of non-alcoholic fatty liver disease. *Signal Transduct Targeted Ther* 2024;**9**:66.
4. Xu X, Poulsen KL, Wu L, Liu S, Miyata T, Song Q, et al. Targeted therapeutics and novel signaling pathways in non-alcohol-associated fatty liver/steatohepatitis (NAFL/NASH). *Signal Transduct Targeted Ther* 2022;**7**:287.
5. Hashim HT, Alhatemi A, Riaz S, Al-Ghuraibawi MA, Alabide AS, Saeed H, et al. Unveiling resmetirom: a systematic review and meta-analysis on its impact on liver function and safety in non-alcoholic steatohepatitis treatment. *JGH Open* 2024;**8**:e70025.
6. Guo P, Li Y, Eslamfam S, Ding W, Ma X. Discovery of novel genes mediating glucose and lipid metabolisms. *Curr Protein Pept Sci* 2017; **18**:609−18.
7. Bhat N, Mani A. Dysregulation of lipid and glucose metabolism in nonalcoholic fatty liver disease. *Nutrients* 2023;**15**:2323.
8. Jones JG. Hepatic glucose and lipid metabolism. *Diabetologia* 2016; **59**:1098−103.
9. Zhao CY, Qu QS, Yang F, Li ZX, Yang PS, Han L, et al. Monascus ruber fermented *Panax ginseng* ameliorates lipid metabolism disorders and modulate gut microbiota in rats fed a high-fat diet. *J Ethnopharmacol* 2021;**278**:114300.
10. Stewart J, Mccallin T, Martinez J, Chacko S, Yusuf S. Hyperlipidemia. *Pediatr Rev* 2020;**41**:393−402.
11. Rodrigues JR, Couto A, Cabezas A, Pinto RM, Ribeiro JM, Canales J, et al. Bifunctional homodimeric triokinase/FMN cyclase: contribution of protein domains to the activities of the human enzyme and molecular dynamics simulation of domain movements. *J Biol Chem* 2014;**289**:10620−36.
12. Helsley RN, Moreau F, Gupta MK, Radulescu A, Debosch B, Softic S. Tissue-specific fructose metabolism in obesity and diabetes. *Curr Diabetes Rep* 2020;**20**:64.
13. Herman MA, Birnbaum MJ. Molecular aspects of fructose metabolism and metabolic disease. *Cell Metab* 2021;**33**:2329−54.
14. Liu L, Li T, Liao Y, Wang Y, Gao Y, Hu H, et al. Triose kinase controls the lipogenic potential of fructose and dietary tolerance. *Cell Metab* 2020;**32**:605−18.
15. Jang C, Hui S, Lu W, Cowan AJ, Morscher RJ, Lee G, et al. The small intestine converts dietary fructose into glucose and organic acids. *Cell Metab* 2018;**27**:351−61.
16. Liput KP, Lepczynski A, Nawrocka A, Polawska E, Ogluszka M, Jonczy A, et al. Effects of three-month administration of high-saturated fat diet and high-polyunsaturated fat diets with different linoleic acid (LA, C18:2n-6) to α-linolenic acid (ALA, C18:3n-3) ratio on the mouse liver proteome. *Nutrients* 2021;**13**:1678.
17. Wen Y, Chen YQ, Konrad RJ. The regulation of triacylglycerol metabolism and lipoprotein lipase activity. *Adv Biol (Weinh)* 2022;**6**: e2200093.
18. Tanigawa K, Hayashi Y, Hama K, Yamashita A, Yokoyama K, Luo Y, et al. *Mycobacterium leprae* promotes triacylglycerol *de novo* synthesis through induction of GPAT3 expression in human premonocytic THP-1 cells. *PLoS One* 2021;**16**:e0249184.
19. Shan D, Li JL, Wu L, Li D, Hurov J, Tobin JF, et al. GPAT3 and GPAT4 are regulated by insulin-stimulated phosphorylation and play distinct roles in adipogenesis. *J Lipid Res* 2010;**51**:1971−81.
20. Karasawa K, Tanigawa K, Harada A, Yamashita A. Transcriptional regulation of acyl-CoA:glycerol-*sn*-3-phosphate acyltransferases. *Int J Mol Sci* 2019;**20**:964.
21. Yu J, Loh K, Song ZY, Yang HQ, Zhang Y, Lin S. Update on glycerol-3-phosphate acyltransferases: the roles in the development of insulin resistance. *Nutr Diabetes* 2018;**8**:34.
22. Farese RJ, Walther TC. Glycerolipid synthesis and lipid droplet formation in the endoplasmic reticulum. *Cold Spring Harbor Perspect Biol* 2023;**15**:a041246.
23. Fan G, Li Y, Zong Y, Suo X, Jia Y, Gao M, et al. GPAT3 regulates the synthesis of lipid intermediate LPA and exacerbates kupffer cell inflammation mediated by the ERK signaling pathway. *Cell Death Dis* 2023;**14**:208.
24. Cao J, Li JL, Li D, Tobin JF, Gimeno RE. Molecular identification of microsomal acyl-CoA:glycerol-3-phosphate acyltransferase, a key enzyme in *de novo* triacylglycerol synthesis. *Proc Natl Acad Sci U S A* 2006;**103**:19695−700.
25. Thota RN, Acharya SH, Garg ML. Curcumin and/or omega-3 polyunsaturated fatty acids supplementation reduces insulin resistance and blood lipids in individuals with high risk of type 2 diabetes: a randomised controlled trial. *Lipids Health Dis* 2019;**18**:31.
26. Saeedi F, Farkhondeh T, Roshanravan B, Amirabadizadeh A, Ashrafizadeh M, Samarghandian S. Curcumin and blood lipid levels: an updated systematic review and meta-analysis of randomised clinical trials. *Arch Physiol Biochem* 2022;**128**:1493−502.
27. Peng Y, Ao M, Dong B, Jiang Y, Yu L, Chen Z, et al. Anti-inflammatory effects of curcumin in the inflammatory diseases: status, limitations and countermeasures. *Drug Des Dev Ther* 2021;**15**: 4503−25.
28. Abrahams S, Haylett WL, Johnson G, Carr JA, Bardien S. Antioxidant effects of curcumin in models of neurodegeneration, aging, oxidative and nitrosative stress: a review. *Neuroscience* 2019;**406**:1−21.
29. Ruiz DPV, Figols M, Font A, Pardina E. Curcumin as a hepatoprotective agent against chemotherapy-induced liver injury. *Life Sci* 2023;**332**:122119.
30. Khajavi M, Shiga K, Wiszniewski W, He F, Shaw CA, Yan J, et al. Oral curcumin mitigates the clinical and neuropathologic phenotype of the Trembler-J mouse: a potential therapy for inherited neuropathy. *Am J Hum Genet* 2007;**81**:438−53.
31. Mirzaei H, Shakeri A, Rashidi B, Jalili A, Banikazemi Z, Sahebkar A. Phytosomal curcumin: a review of pharmacokinetic, experimental and clinical studies. *Biomed Pharmacother* 2017;**85**:102−12.
32. Kang OH, Kim SB, Seo YS, Joung DK, Mun SH, Choi JG, et al. Curcumin decreases oleic acid-induced lipid accumulation *via* AMPK phosphorylation in hepatocarcinoma cells. *Eur Rev Med Pharmacol Sci* 2013;**17**:2578−86.
33. Nosrati-Oskouie M, Aghili-Moghaddam NS, Sathyapalan T, Sahebkar A. Impact of curcumin on fatty acid metabolism. *Phytother Res* 2021;**35**:4748−62.
34. Molani-Gol R, Dehghani A, Rafraf M. Effects of curcumin/turmeric supplementation on the liver enzymes, lipid profiles, glycemic index, and anthropometric indices in non-alcoholic fatty liver patients: an umbrella meta-analysis. *Phytother Res* 2024;**38**:539−55.
35. Ngu MH, Norhayati MN, Rosnani Z, Zulkifli MM. Curcumin as adjuvant treatment in patients with non-alcoholic fatty liver (NAFLD) disease: a systematic review and meta-analysis. *Compl Ther Med* 2022;**68**:102843.
36. Liou CJ, Wu SJ, Shen SC, Chen LC, Chen YL, Huang WC. Phloretin ameliorates hepatic steatosis through regulation of lipogenesis and SIRT1/AMPK signaling in obese mice. *Cell Biosci* 2020;**10**:114.
37. Sattlegger E, Wiedemann M, Lee SJ, Silva RCD, Visweswaraiah J, Soppert J. *Simultaneous semi-dry electrophoretic transfer of a wide range of differently sized proteins for immunoblotting*. V.1. Protocols.io; 2013. Available from: https://doi.org/10.1038/protex.2013.095.

38. Sule R, Rivera G, Gomes AV. Western blotting (immunoblotting): history, theory, uses, protocol and problems. *Biotechniques* 2023;**75**: 99−114.
39. Liao LX, Song XM, Wang LC, Lv HN, Chen JF, Liu D, et al. Highly selective inhibition of IMPDH2 provides the basis of anti-neuroinflammation therapy. *Proc Natl Acad Sci U S A* 2017;**114**: E5986−94.
40. Dai J, Liang K, Zhao S, Jia W, Liu Y, Wu H, et al. Chemoproteomics reveals baicalin activates hepatic CPT1 to ameliorate diet-induced obesity and hepatic steatosis. *Proc Natl Acad Sci U S A* 2018;**115**: E5896−905.
41. Liu W, Li Z, Chu S, Ma X, Wang X, Jiang M, et al. Atractylenolide-I covalently binds to CYP11B2, selectively inhibits aldosterone synthesis, and improves hyperaldosteronism. *Acta Pharm Sin B* 2022;**12**: 135−48.
42. Chen C, Gong L, Liu X, Zhu T, Zhou W, Kong L, et al. Identification of peroxiredoxin 6 as a direct target of withangulatin a by quantitative chemical proteomics in non-small cell lung cancer. *Redox Biol* 2021; **46**:102130.
43. Wang LC, Liao LX, Lv HN, Liu D, Dong W, Zhu J, et al. Highly selective activation of heat shock protein 70 by allosteric regulation provides an insight into efficient neuroinflammation inhibition. *EBioMedicine* 2017;**23**:160−72.
44. Zhang J, Luan ZL, Huo XK, Zhang M, Morisseau C, Sun CP, et al. Direct targeting of sEH with alisol B alleviated the apoptosis, inflammation, and oxidative stress in cisplatin-induced acute kidney injury. *Int J Biol Sci* 2023;**19**:294−310.
45. Chen X, Wong YK, Wang J, Zhang J, Lee YM, Shen HM, et al. Target identification with quantitative activity based protein profiling (ABPP). *Proteomics* 2017;**17**:e1600212.
46. Wang J, Gao L, Lee YM, Kalesh KA, Ong YS, Lim J, et al. Target identification of natural and traditional medicines with quantitative chemical proteomics approaches. *Pharmacol Ther* 2016;**162**:10−22.
47. Ji H, Dong H, Lan Y, Bi Y, Gu X, Han Y, et al. Metformin attenuates fibroblast activation during pulmonary fibrosis by targeting S100A4 *via* AMPK−STAT3 axis. *Front Pharmacol* 2023;**14**:1089812.
48. Hassan FE, Aboulhoda BE, Mehesen MN, El DP, Abdallah HA, Bendas ER, et al. Combination therapy of systemic and local metformin improves imiquimod-induced psoriasis-like lesions with type 2 diabetes: the role of AMPK/KGF/STAT3 axis. *Arch Physiol Biochem* 2025;**131**:252−64.
49. Zhou Y, Zhao H, Ren R, Zhou M, Zhang J, Wu Z, et al. GPAT3 is a potential therapeutic target to overcome sorafenib resistance in hepatocellular carcinoma. *Theranostics* 2024;**14**:3470−85.
50. Kasprzak-Drozd K, Oniszczuk T, Gancarz M, Kondracka A, Rusinek R, Oniszczuk A. Curcumin and weight loss: does it work?. *Int J Mol Sci* 2022;**23**:639.
51. Baker M. Deceptive curcumin offers cautionary tale for chemists. *Nature* 2017;**541**:144−5.
52. Heger M. Drug screening: don't discount all curcumin trial data. *Nature* 2017;**543**:40.
53. Samuel VT, Shulman GI. Nonalcoholic fatty liver disease as a nexus of metabolic and hepatic diseases. *Cell Metab* 2018;**27**:22−41.
54. Preuss C, Jelenik T, Bodis K, Mussig K, Burkart V, Szendroedi J, et al. A new targeted lipidomics approach reveals lipid droplets in liver, muscle and heart as a repository for diacylglycerol and ceramide species in non-alcoholic fatty liver. *Cells* 2019;**8**:277.
55. Li TY, Song L, Sun Y, Li J, Yi C, Lam SM, et al. Tip60-mediated lipin 1 acetylation and ER translocation determine triacylglycerol synthesis rate. *Nat Commun* 2018;**9**:1916.
56. Wu L, Xu D, Zhou L, Xie B, Yu L, Yang H, et al. Rab8a−AS160−MSS4 regulatory circuit controls lipid droplet fusion and growth. *Dev Cell* 2014;**30**:378−93.
57. Chen S, Huang Y, Su H, Zhu W, Wei Y, Long Y, et al. The integrated analysis of transcriptomics and metabolomics unveils the therapeutical effect of asiatic acid on alcoholic hepatitis in rats. *Inflammation* 2022; **45**:1780−99.
58. Ding Q, Guo R, Pei L, Lai S, Li J, Yin Y, et al. *N*-Acetylcysteine alleviates high fat diet-induced hepatic steatosis and liver injury *via* regulating the intestinal microecology in mice. *Food Funct* 2022;**13**: 3368−80.
59. Liu CX, Yin QQ, Zhou HC, Wu YL, Pu JX, Xia L, et al. Adenanthin targets peroxiredoxin I and II to induce differentiation of leukemic cells. *Nat Chem Biol* 2012;**8**:486−93.
60. Lv C, Huang Y, Wang Q, Wang C, Hu H, Zhang H, et al. Ainsliadimer a induces ROS-mediated apoptosis in colorectal cancer cells *via* directly targeting peroxiredoxin 1 and 2. *Cell Chem Biol* 2023;**30**: 295−307.
61. Dong T, Li C, Wang X, Dian L, Zhang X, Li L, et al. Ainsliadimer a selectively inhibits IKKα/β by covalently binding a conserved cysteine. *Nat Commun* 2015;**6**:6522.
62. Wei W, Zeng Q, Wang Y, Guo X, Fan T, Li Y, et al. Discovery and identification of EIF2AK2 as a direct key target of berberine for anti-inflammatory effects. *Acta Pharm Sin B* 2023;**13**:2138−51.
63. Chen X, Wang Y, Ma N, Tian J, Shao Y, Zhu B, et al. Target identification of natural medicine with chemical proteomics approach: probe synthesis, target fishing and protein identification. *Signal Transduct Targeted Ther* 2020;**5**:72.
64. Sun CP, Zhou JJ, Yu ZL, Huo XK, Zhang J, Morisseau C, et al. Kurarinone alleviated Parkinson's disease *via* stabilization of epoxyeicosatrienoic acids in animal model. *Proc Natl Acad Sci U S A* 2022; **119**:e2118818119.
65. Kong LM, Deng X, Zuo ZL, Sun HD, Zhao QS, Li Y. Identification and validation of p50 as the cellular target of eriocalyxin B. *Oncotarget* 2014;**5**:11354−64.
66. Xu J, Li X, Ding K, Li Z. Applications of activity-based protein profiling (ABPP) and bioimaging in drug discovery. *Chem Asian J* 2020;**15**:34−41.
67. Yuan J, Dong X, Yap J, Hu J. The MAPK and AMPK signalings: interplay and implication in targeted cancer therapy. *J Hematol Oncol* 2020;**13**:113.
68. Lempesis IG, van Meijel R, Manolopoulos KN, Goossens GH. Oxygenation of adipose tissue: a human perspective. *Acta Physiol* 2020;**228**:e13298.
69. Shigeta T, Sasamoto K, Yamamoto T. Glyceraldehyde-derived advanced glycation end-products having pyrrolopyridinium-based crosslinks. *Biochem Biophys Rep* 2021;**26**:100963.
70. Priyadarsini KI. The chemistry of curcumin: from extraction to therapeutic agent. *Molecules* 2014;**19**:20091−112.
71. Steinberg GR, Hardie DG. New insights into activation and function of the AMPK. *Nat Rev Mol Cell Biol* 2023;**24**:255−72.
72. Smiles WJ, Ovens AJ, Oakhill JS, Kofler B. The metabolic sensor AMPK: twelve enzymes in one. *Mol Metabol* 2024;**90**:102042.
73. Reilly SM, Hung CW, Ahmadian M, Zhao P, Keinan O, Gomez AV, et al. Catecholamines suppress fatty acid re-esterification and increase oxidation in white adipocytes *via* STAT3. *Nat Metab* 2020;**2**: 620−34.
74. Reilly S, Aksu A, Zerbel Z, Dhillon P, Kelemen Y, Gbayisomore O, et al. Fatty acids promote uncoupled respiration *via* the ATP/ADP carrier in white adipocytes. *Res Sq* 2024. rs.3.rs-5094089.